One- versus two-pole $\bar{K}N$-$\pi\Sigma$ potential: K^-d scattering length

N. V. Shevchenko
Nuclear Physics Institute, 25068 Řež, Czech Republic
(Received 25 March 2011; revised manuscript received 31 January 2012; published 6 March 2012)

We investigated the dependence of the K^-d scattering length on models of the $\bar{K}N$ interaction with one or two poles for the $\Lambda(1405)$ resonance. The $\bar{K}NN$-$\pi\Sigma N$ system is described by coupled-channel Faddeev equations in Alt-Grassberger-Sandhas form. Our new two-body $\bar{K}N$-$\pi\Sigma$ potentials reproduce all existing experimental data on K^-p scattering and kaonic hydrogen atom characteristics. New models of the ΣN-ΛN interaction were also constructed. Comparison with several approximations, usually used for scattering length calculations, was performed.

DOI: 10.1103/PhysRevC.85.034001 PACS number(s): 13.75.Jz, 11.80.Gw, 14.20.Gk, 21.45.−v

I. INTRODUCTION

Investigation of the K^-d system can shed more light on the $\bar{K}N$ interaction, necessary for the study of antikaonic nuclear clusters, which has attracted large interest recently [1]. The interaction is not very well known; in particular, there are debates about the nature of the $\Lambda(1405)$ resonance. The question is whether it is a single resonance in $\pi\Sigma$ and a quasibound state in the $\bar{K}N$ channel or whether the bump, which is usually understood as the $\Lambda(1405)$ resonance, is an effect of two poles. The advantage of the K^-d system is the possibility of obtaining a proper description of its dynamics using Faddeev equations [2].

Recently, we constructed coupled-channel $\bar{K}N$-$\pi\Sigma$ potentials in one- and two-pole form [3], which reproduce all existing experimental data on K^-p scattering and K^-p atom characteristics equally well; therefore it is not possible to give preference to any of the versions. A possible way to clarify the question concerning the nature of the $\Lambda(1405)$ resonance is to perform few- or many-body calculations using one- and two-pole $\bar{K}N$-$\pi\Sigma$ potentials as an input. Keeping in mind the SIDDHARTA experiment [4], in which characteristics of the kaonic deuterium atom are measured, we calculated the K^-d scattering length a_{K^-d} and investigated the dependence of the results on the models of the $\bar{K}N$ interaction with the newly obtained parameters. The scattering length makes it possible to calculate the kaonic deuterium level shift and width. Comparison of the theoretical results with experimental ones could allow us to choose between the two $\bar{K}N$-$\pi\Sigma$ interaction versions.

The dependence of a_{K^-d} on other two-body interactions, necessary for the description of the $\bar{K}NN$-$\pi\Sigma N$ system, was also investigated: we used several models of NN (with and without short-range repulsion) and ΣN(-ΛN) interactions. In addition to the full coupled-channel calculation we performed checks of commonly used approximations for K^-d scattering. In particular, we solved one-channel Faddeev equations using exact optical and simple complex $\bar{K}N$ potentials approximating the $\bar{K}N$-$\pi\Sigma$ models of interaction. We also checked the "fixed-center approximation to the Faddeev equations" formula.

The formalism used for the coupled-channel K^-d scattering length calculation is described in the next section. Section III is devoted to the two-body input: the description of the one- and two-pole $\bar{K}N$-$\pi\Sigma$ potentials with newly obtained parameters in the first subsection is supplemented with additional arguments for equivalence of the two versions. The following subsections of Sec. III are devoted to NN and ΣN-ΛN potentials. Section IV contains information about approximate methods usually used in K^-d scattering length calculations. The full and approximate results are shown and discussed in Sec. V, while Sec. VI concludes the paper.

II. COUPLED-CHANNEL ALT-GRASSBERGER-SANDHAS EQUATIONS FOR THE $\bar{K}NN$-$\pi\Sigma N$ SYSTEM

As in Refs. [5,6] we directly include the $\pi\Sigma N$ channel into the original three-body Faddeev equations in the Alt-Grassberger-Sandhas (AGS) form [7], which leads to the coupled-channel equations

$$U_{ij}^{\alpha\beta} = \delta_{\alpha\beta}\,(1-\delta_{ij})\,\left(G_0^{\alpha}\right)^{-1} + \sum_{k,\gamma=1}^{3}(1-\delta_{ik})\,T_k^{\alpha\gamma}\,G_0^{\gamma}\,U_{kj}^{\gamma\beta}, \tag{1}$$

where "particle channel" indices $\alpha, \beta = 1, 2, 3$ are introduced in addition to the usual Faddeev partition indices $i, j, k = 1, 2, 3$ (see Table I). The equations define unknown operators $U_{ij}^{\alpha\beta}$, describing the elastic and rearrangement processes $j^\beta + (k^\beta i^\beta) \to i^\alpha + (j^\alpha k^\alpha)$. The free Green's function is diagonal in channel indices: $G_0^{\alpha\beta} = \delta_{\alpha\beta}\,G_0^{\alpha}$. The inputs for the system of equations (1) are two-body T matrices, embedded into three-body space: $T_i^{\alpha\beta}$ describes the interaction between particles j and k ($i \neq j \neq k$) in channels α, β. Like in Ref. [6], here we have T_i^{NN}, $T_i^{\pi N}$, and $T_i^{\Sigma N}$, which are the usual one-channel two-body T matrices in three-body space, describing NN, πN, and ΣN interactions, respectively. The T_i^{KK}, $T_i^{\pi\pi}$, $T_i^{\pi K}$, and $T_i^{K\pi}$ are elements of the coupled-channel T matrix for the $\bar{K}N$-$\pi\Sigma$ system.

In contrast to the calculation of the quasibound K^-pp state [6], where one-term isospin (I) dependent separable potentials were used, now we write the AGS equations for

TABLE I. Interacting two-body subsystems for three partition (i) and three particle-channel (α) indices. Possible values of the two-body isospins (I) are also shown.

$i \setminus \alpha$	1 ($\bar{K}NN$)	2 ($\pi\Sigma N$)	3 ($\pi N\Sigma$)
1	$NN_{I=0,1}$	$\Sigma N_{I=\frac{1}{2},\frac{3}{2}}$	$\Sigma N_{I=\frac{1}{2},\frac{3}{2}}$
2	$\bar{K}N_{I=0,1}$	$\pi N_{I=\frac{1}{2},\frac{3}{2}}$	$\pi\Sigma_{I=0,1}$
3	$\bar{K}N_{I=0,1}$	$\pi\Sigma_{I=0,1}$	$\pi N_{I=\frac{1}{2},\frac{3}{2}}$

N-term isospin-dependent separable potentials

$$V_{i,I}^{\alpha\beta} = \sum_{m=1}^{N_i^\alpha} \lambda_{i(m),I}^{\alpha\beta} \left|g_{i(m),I}^{\alpha}\right\rangle\left\langle g_{i(m),I}^{\beta}\right|, \tag{2}$$

which lead to separable T matrices

$$T_{i,I}^{\alpha\beta} = \sum_{m,n=1}^{N_i^\alpha} \left|g_{i(m),I}^{\alpha}\right\rangle \tau_{i(mn),I}^{\alpha\beta} \left\langle g_{i(n),I}^{\beta}\right|. \tag{3}$$

Here N_i^α is the number of terms of the separable potential, λ is a strength constant, while g is a form factor. The bound-state wave function of the two-body subsystem, described by such a potential, has the form

$$\left|\psi_{i,I}^{\alpha}\right\rangle = \sum_{m=1}^{N_i^\alpha} C_{i(m),I}^{\alpha}\, G_0^\alpha(z_{\rm bnd}) \left|g_{i(m),I}^{\alpha}\right\rangle, \tag{4}$$

where the coefficients $C_{i(m),I}^{\alpha}$ are constants and $|z_{\rm bnd}|$ is a binding energy. We used two slightly different versions of a two-term nucleon-nucleon separable potential ($N_i^\alpha = 2$) in the a_{K^-d} calculations. All other models of interactions, one more V^{NN} among them, are one-term potentials with $N_i^\alpha = 1$.

The amplitude $f_{ij,I_iI_j}^{\alpha\beta}$ of the $\bar{K}(NN) \to \bar{K}(NN)$ reaction with NN in the isospin-zero state in the initial and final states is defined by the following matrix element:

$$\begin{aligned} &f_{11,00}^{11}\left(\vec{p}_1^{\,1}, \vec{p}^{\,\prime}{}_1^{\,1}; z_{\rm tot}\right) \\ &\quad = -(2\pi)^2\, \mu_1^1 \left\langle \vec{p}_1^{\,1}; \psi_{1,0}^1 \right| U_{11,00}^{11}(z_{\rm tot}) \left|\psi_{1,0}^1; \vec{p}^{\,\prime}{}_1^{\,1}\right\rangle, \end{aligned} \tag{5}$$

where μ_i^α is the three-body reduced mass defined by

$$\mu_i^\alpha = \frac{m_i^\alpha\left(m_j^\alpha + m_k^\alpha\right)}{m_i^\alpha + m_j^\alpha + m_k^\alpha}, \quad i \neq j \neq k, \tag{6}$$

$\vec{p}_1^{\,1}$ and $\vec{p}^{\,\prime}{}_1^{\,1}$ are initial and final relative momenta of the antikaon with respect to the NN pair, correspondingly, while z_{tot} is the total energy of the three-body system. The deuteron wave function $\psi_{1,0}^1$ in Eq. (5) is defined by Eq. (4), and the transition operator $U_{ij,I_iI_j}^{\alpha\beta}$ has two additional isospin indices compared to Eq. (1). The scattering length is the amplitude at zero kinetic energy of relative K^--d motion:

$$a_{K^-d} = f_{11,00}^{11}\left(\vec{p}_1^{\,1} \to 0, \vec{p}^{\,\prime}{}_1^{\,1} \to 0; z_{\rm tot} \to z_{\rm th}^1 + z_{\rm bnd}\right), \tag{7}$$

with $z_{\rm th}^\alpha = \sum_{i=1}^3 m_i^\alpha$ being the $\bar{K}NN$ ($\alpha = 1$) or $\pi\Sigma N$ ($\alpha = 2$) threshold energy; $|z_{\rm bnd}|$ here is the binding energy of the deuteron.

Taking into account forms of T matrices (3) and wave functions (4), introducing new operators

$$X_{i(m)j,I_iI_j}^{\alpha\beta} \equiv \left\langle g_{i(m),I_i}^{\alpha}\right| G_0^\alpha\, U_{ij,I_iI_j}^{\alpha\beta} \left|\psi_{j,I_j}^{\beta}\right\rangle, \tag{8}$$

$$\begin{aligned} Z_{i(m)j(n),I_iI_j}^{\alpha\beta} &\equiv \delta_{\alpha\beta}\, Z_{i(m)j(n),I_iI_j}^{\alpha} \\ &= \delta_{\alpha\beta}\,(1-\delta_{ij}) \left\langle g_{i(m),I_i}^{\alpha}\right| G_0^\alpha \left|g_{j(n),I_j}^{\alpha}\right\rangle, \end{aligned} \tag{9}$$

and substituting them into the system (1), we can write a system of equations for the new unknown operators $X_{ij,I_iI_j}^{\alpha\beta}$:

$$\begin{aligned} X_{i(l)j,I_iI_j}^{\alpha\beta} &= \delta_{\alpha\beta} \sum_{m=1}^{N_j^\alpha} C_{j(m)}^{\alpha}\, Z_{i(l)j(m),I_iI_j}^{\alpha} \\ &\quad + \sum_{k,\gamma=1}^{3} \sum_{m,n=1}^{N_k^\alpha} \sum_{I_k} Z_{i(l)k(m),I_iI_k}^{\alpha}\, \tau_{k(mn),I_k}^{\alpha\gamma}\, X_{k(n)j,I_kI_j}^{\gamma\beta}. \end{aligned} \tag{10}$$

The number of equations in the system (10) is defined by the number of all form factors g. Therefore, the system (10) with a two-term NN and one-term other potentials consists of 20 equations.

Two identical nucleons, entering the first ($\bar{K}NN$) channel, require antisymmetrization of the system of equations. The orbital angular momentum of all two-body interactions was set to zero. The main $\bar{K}N$-$\pi\Sigma$ potential was constructed with orbital angular momentum $l = 0$ since the interaction is dominated by the s-wave $\Lambda(1405)$ resonance. The interaction of the π meson with the nucleon is mainly in the p wave; however, as was shown in Ref. [8], the addition of "small two-body interactions," πN among them, changes the resulting a_{K^-d} very slightly (of the order of 1% or even less; see Table XIII of Ref. [8]). On the other hand, the s-wave πN interaction is even weaker; therefore, we omitted the πN interaction in our equations. Information on the ΣN interaction is very poor, and there is no reason to assume a significant effect of higher partial waves. Finally, theNN interaction was also taken in the $l = 0$ state only since we do not see physical reasons for a sufficient effect of higher partial waves in the present calculation.

The antisymmetric s-wave deuteron wave function has zero isospin and spin equal to one. Due to this, the K^-d system, in contrast to K^-pp [5,6], has a total three-body spin (and total angular momentum) equal to one, while both $\bar{K}NN$ systems have total isospin $I = \frac{1}{2}$. Therefore, in the K^-d case, antisymmetrization leads to the following new operators:

$$\begin{aligned} X_{1(m),0}^{1,\rm asm} &= X_{1(m),0}^{1}, & X_{2,I}^{1,\rm asm} &= X_{2,I}^{1} - X_{3,I}^{1}, \\ X_{1,\frac{1}{2}}^{2,\rm asm} &= X_{1,\frac{1}{2}}^{2} + X_{1,\frac{1}{2}}^{3}, & X_{1,\frac{3}{2}}^{2,\rm asm} &= X_{1,\frac{3}{2}}^{2} - X_{1,\frac{3}{2}}^{3}, \\ X_{2,I}^{2,\rm asm} &= X_{2,I}^{2} - X_{3,I}^{3}, & X_{3,I}^{2,\rm asm} &= X_{3,I}^{2} - X_{2,I}^{3}. \end{aligned} \tag{11}$$

It is necessary to note that the $\bar{K}^0nn$ state drops out from the system of equations (10) after the antisymmetrization because the two neutrons are in an isospin one state. Therefore the $\bar{K}^0nn$ channel has another value of the three-body spin ($S = 0$) than K^-d ($S = 1$) or the neutrons do not satisfy Pauli principle.

Finally, the K^-d scattering length can be found from

$$a_{K^-d} = -(2\pi)^2 \mu_1^1 \sum_{m=1}^{2} C^1_{1(m),0} X^{1,\mathrm{asm}}_{1(m),0}(0,0;z^1_{\mathrm{th}}). \quad (12)$$

The system of operator equations (10) written in momentum space turns into a system of integral equations. In order to solve the inhomogeneous system we transformed the integral equations into algebraic ones. It is known (see, e.g., [9]) that the integral Faddeev equations have moving logarithmic singularities in the kernels when scattering above a three-body breakup threshold ($z_{\mathrm{tot}} > z_{\mathrm{th}}$) is described. "Usual" (one-channel) scattering length calculations are free of the singularities. For the $\bar{K}NN$-$\pi\Sigma N$ system, however, where $z^2_{\mathrm{th}} < z^1_{\mathrm{th}}$, the permanently opened $\pi\Sigma N$ channel causes the appearance of logarithmic singularities in K^-d scattering length calculations. In the numerical procedure we handle them using the method suggested in Ref. [10]. The main idea of the method consists in interpolating the unknown solutions (in the interval containing the singular points) by certain polynomials and subsequent analytic integration of the singular part of the kernels.

III. TWO-BODY INPUT

The separable $\bar{K}N$-$\pi\Sigma$, NN, and ΣN potentials (2) in momentum representation have the form

$$V_I^{\bar{\alpha}\bar{\beta}}(k^{\bar{\alpha}}, k'^{\bar{\beta}}) = \sum_{m=1}^{N^{\bar{\alpha}}} \lambda^{\bar{\alpha}\bar{\beta}}_{(m),I}\; g^{\bar{\alpha}}_{(m),I}(k^{\bar{\alpha}})\, g^{\bar{\beta}}_{(m),I}(k'^{\bar{\beta}}). \quad (13)$$

Here for convenience new indices of two-body channels $\bar{\alpha}, \bar{\beta} = 1, 2$ were introduced. Correspondence between a two-body index $\bar{\alpha}$ and a pair (α, i) of the three-body channel and Faddeev indices, defining an interacting pair, can be established with the help of Table I. As before, $N^{\bar{\alpha}}$ defines the number of terms of the potential. As was already stated, we neglected here the πN interaction due to its smallness.

In addition to the coupled-channel potentials [Eq. (13) with $\bar{\alpha}, \bar{\beta} > 1$] we used optical and complex one-channel potentials corresponding to them. Noting that nowadays many authors misuse the term "optical" to a complex potential, we will call our one-channel potentials "exact optical" and "simple complex." An exact optical potential by definition reproduces the elastic part of the coupled-channel interaction exactly. In particular, the imaginary part of the corresponding amplitude becomes zero below the lowest channel threshold.

The exact optical one-channel potential, corresponding to a two-channel V (with $N^{\bar{\alpha}} = 1$), is given by Eq. (13) with $\bar{\alpha}, \bar{\beta} = 1$ and the strength parameter defined as

$$\lambda_I^{11,\mathrm{Opt}} = \lambda_I^{11} + \frac{\left(\lambda_I^{12}\right)^2 \left\langle g_I^2\right| G_0^{(2)}(z^{(2)}) \left|g_I^2\right\rangle}{1 - \lambda_I^{22} \left\langle g_I^2\right| G_0^{(2)}(z^{(2)}) \left|g_I^2\right\rangle}, \quad (14)$$

where $\lambda_I^{\bar{\alpha},\bar{\beta}}$ are strength parameters of the two-channel potential and $|g_I^2\rangle$ is the form factor of the second channel. Keeping in mind that the two-body free Green's function $G_0^{(2)}$ depends on the corresponding two-body energy $z^{(2)}$, we see that $\lambda_I^{11,\mathrm{Opt}}$ of the exact optical potential is an energy-dependent complex function. In contrast to it, a strength parameter $\lambda_I^{11,\mathrm{Complex}}$ of a simple complex potential is a complex constant, and, therefore, the simple complex potential is energy independent. The strength parameter of a simple complex potential is chosen in such a way that the potential reproduces some characteristics of the full interaction, say, scattering lengths. Exact optical and simple complex potentials take into account flux losses into inelastic channels through imaginary parts of the strength parameters.

A. $\bar{K}N$-$\pi\Sigma$ potential

Two versions of the phenomenological coupled-channel $\bar{K}N$-$\pi\Sigma$ potential, constructed in Ref. [3], have one- and two-pole forms of the $\Lambda(1405)$ resonance and simultaneously reproduce all existing experimental data. In the present work we performed new fits of the experimental data with the same potential forms. The one-term ($N^{\bar{\alpha}} = 1$) two-channel potential is defined by Eq. (13), where $\bar{\alpha} = 1$ denotes the $\bar{K}N$, and $\bar{\alpha} = 2$ denotes the $\pi\Sigma$ channel. All physical values for data fitting were obtained by solving coupled-channel Lippmann–Schwinger equations with direct inclusion of the Coulomb potential into the K^-p system. Another source of isospin symmetry breaking is the use of physical masses for K^-, $\bar{K}^0$, p, and n.

In comparison to [3], where one one-pole and one two-pole potentials were constructed, here we obtained two sets of potential parameters $\lambda_I^{\bar{\alpha}\bar{\beta}}$ and $\beta_I^{\bar{\alpha}}$: one set for the one-pole structure and another for two-pole structure of the $\Lambda(1405)$ resonance. Each potential of these sets gives a medium value for the threshold branching ratios [11,12]:

$$\gamma = 2.36 \pm 0.04, \quad (15)$$

$$R_{\pi\Sigma} = 0.709 \pm 0.011, \quad (16)$$

where the second is a new ratio, constructed from experimentally measured R_c and R_n:

$$R_{\pi\Sigma} = \frac{R_c}{1 - R_n\,(1 - R_c)}. \quad (17)$$

In contrast to R_c and R_n, the new branching ratio $R_{\pi\Sigma}$ does not contain the $\pi^0\Lambda$ channel, which is taken into account in our formalism only effectively through the nonzero imaginary part of the $\lambda_1^{\bar{K}\bar{K}}$ parameter.

Elastic and inelastic K^-p cross sections $K^-p \to K^-p$, $K^-p \to \bar{K}^0n$, $K^-p \to \pi^+\Sigma^-$, $K^-p \to \pi^-\Sigma^+$, and $K^-p \to \pi^0\Sigma^0$ are properly reproduced by our new potentials as well. The theoretical results together with experimental data [13–17] are shown in Figs. 1 and 2 for one- and two-pole sets of potentials, respectively (in which we did not take into consideration data from [18] with huge error bars). The potentials within each set provide slightly different cross sections, which results in a band instead of a line in the figures. In the same way as in Ref. [3] we defined the "total elastic" K^-p cross section as an integral of the differential cross section over the $-1 \leqslant \cos\theta \leqslant 0.966$ region due to the singularity of the pure Coulomb transition matrix in the forward direction.

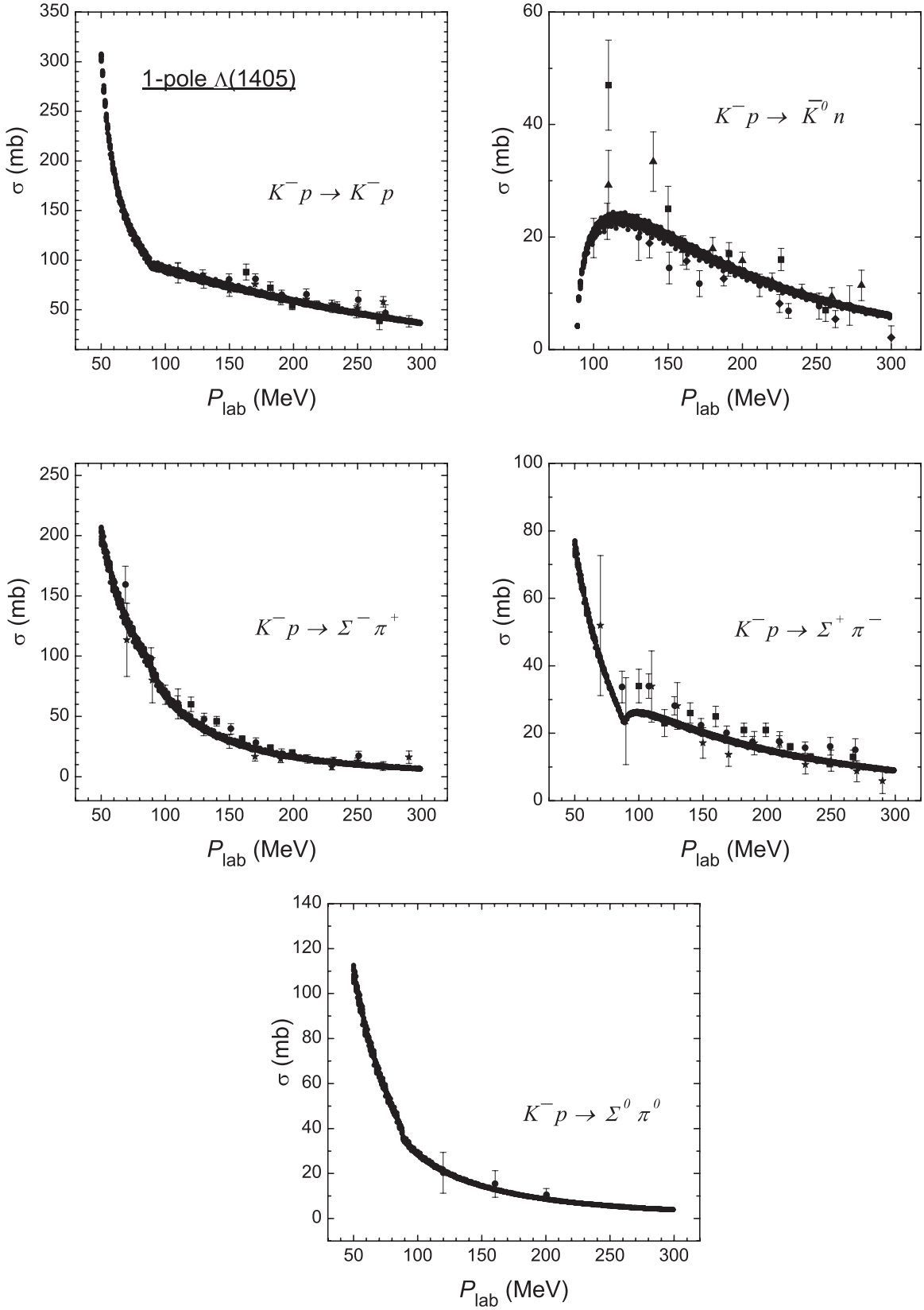

FIG. 1. Comparison of the elastic and inelastic $K^- p$ cross sections (filled circles) for the one-pole sets of the $\bar{K}N$-$\pi\Sigma$ potential with experimental data [13–17] (data points). The theoretical bands are formed by all lines obtained with individual potentials within the set.

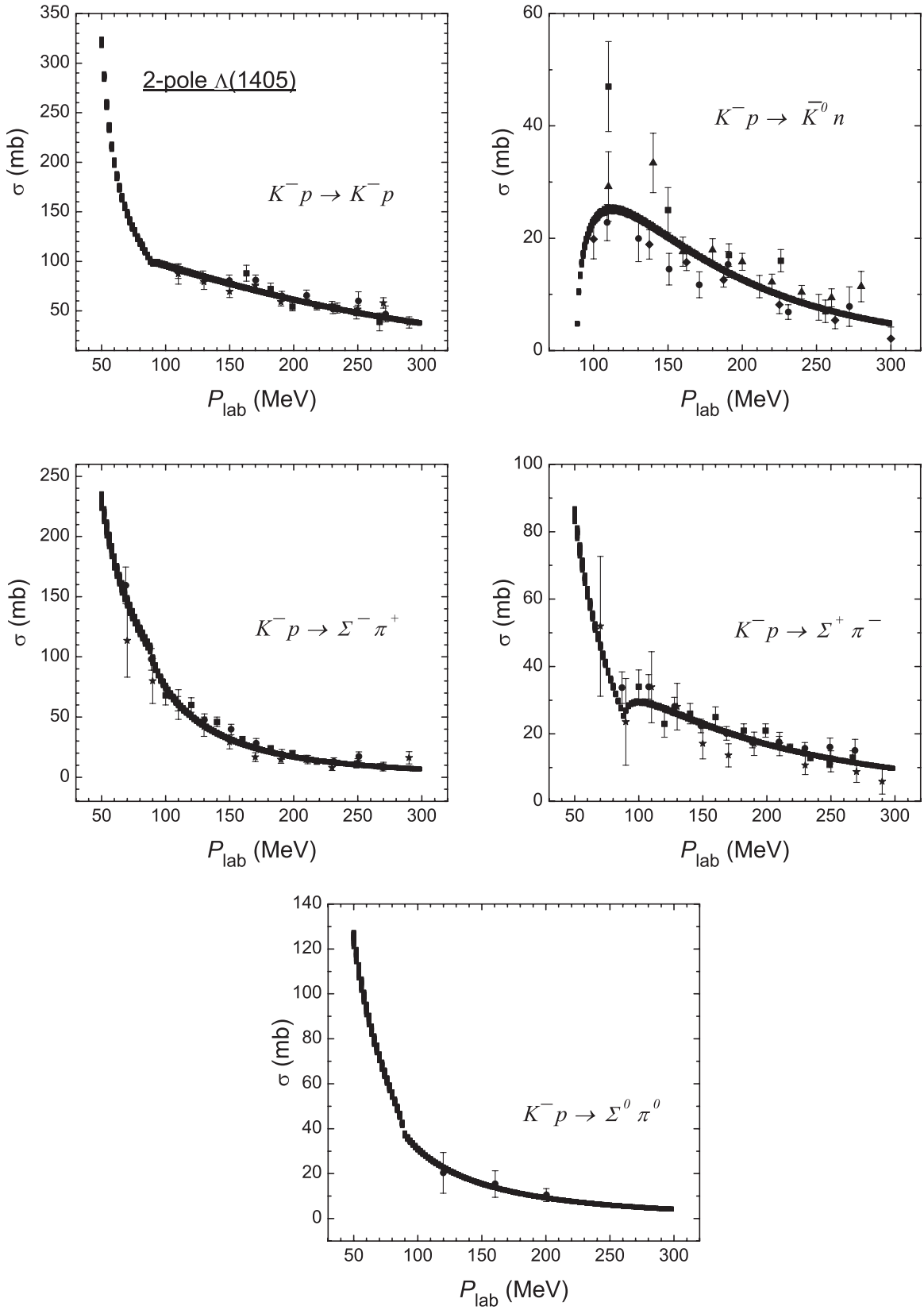

FIG. 2. Comparison of the elastic and inelastic $K^- p$ cross sections (filled circles) for the two-pole sets of the $\bar{K}N$-$\pi\Sigma$ potential with experimental data [13–17] (data points). The theoretical bands are formed by all lines obtained with individual potentials within the set.

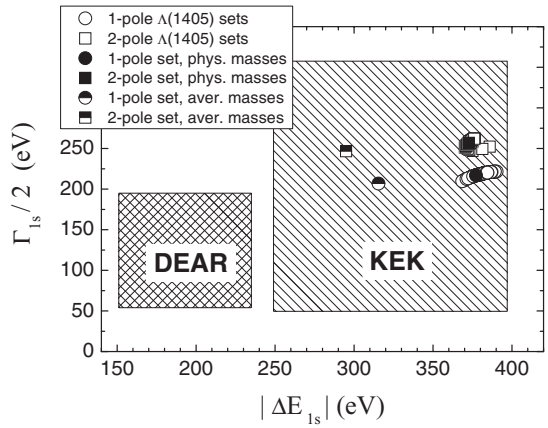

FIG. 3. Kaonic hydrogen $1s$ level shift $|\Delta E|$ (absolute value) and width Γ values for the one-pole (empty circles) and two-pole (empty squares) sets of the $\bar{K}N$-$\pi\Sigma$ potential. Filled circle and filled square denote the results for the one- and two-pole representative potentials, correspondingly, obtained with physical masses. The same kaonic hydrogen observables calculated with averaged masses are denoted by half-empty circle and square. Experimental DEAR and KEK 1σ confidence regions are also shown.

The characteristics of the kaonic hydrogen atom $(\Delta E_{1s}, \Gamma_{1s})$ provided by our potentials are situated within 1σ region of the KEK [19] experiment (see Fig. 3). Experimental results obtained by the DEAR Collaboration [20] are also shown.[1]

A typical resonance behavior manifests itself in the $\pi^0\Sigma^0$ elastic cross sections, corresponding to one- and two-pole sets of the $\bar{K}N$-$\pi\Sigma$ potential (bands, consisting of individual lines; see Fig. 4). All resonance maxima are situated near Particle Data Group (PDG) [22] values for the $\Lambda(1405)$ resonance mass and width:

$$M^{\rm PDG}_{\Lambda(1405)} = 1406.5 \pm 4.0 \text{ MeV}, \quad \Gamma^{\rm PDG}_{\Lambda(1405)} = 50 \pm 2.0 \text{ MeV}. \tag{18}$$

The PDG mass of the $\Lambda(1405)$ resonance is also shown in the figures. Strong pole positions and widths are slightly different for the potentials within one- and two-pole sets of potentials.

For a more detailed description of the properties of our models of the $\bar{K}N$-$\pi\Sigma$ interaction we chose two "representative" potentials: one with a one-pole structure and another with a two-pole structure of the $\Lambda(1405)$ resonance. The parameters of the potentials are shown in Table II, and the corresponding observables are listed in Table III. The latter contains the above-mentioned γ, $R_{\pi\Sigma}$ ratios, and kaonic hydrogen characteristics ΔE_{1s} and Γ_{1s} together with positions of the strong poles z_1 and z_2. Potentials with equal z_1 values were chosen as representative ones. The strong K^-p scattering lengths a_{K^-p}, exactly corresponding to the kaonic hydrogen observables, are shown in Table III. Since both a_{K^-p} and $(\Delta E_{1s}, \Gamma_{1s})$ were obtained by exact solution of the Lippmann-Schwinger equation, the relation between them does not correspond to any commonly used approximate formula. From Figs. 1–3 and Table III it is seen that our new one- and two-pole $\bar{K}N$-$\pi\Sigma$ potentials reproduce all experimental data within experimental errors indistinguishably well in the same way as the ones in Ref. [3]. Therefore it is not possible to give preference to either of the two versions.

In addition, we checked several arguments, which were presented in support of the idea of the two-pole structure of the $\Lambda(1405)$ resonance. One of them is the difference among charged $\pi\Sigma$ cross sections seen in different experiments, such as CLAS [23]. In order to check the assumption, that the difference is caused by the two-pole structure, we plotted $\pi^+\Sigma^-$, $\pi^-\Sigma^+$, and $\pi^0\Sigma^0$ elastic cross sections. The result is seen in Fig. 5: the cross sections are different and their maxima are shifted with respect to each another for both one- and two-pole versions of the $\bar{K}N$-$\pi\Sigma$ potential. Therefore, it is not a proof of the two-pole structure but a manifestation of an isospin-breaking effect and different background.

Another argument for two-pole structure comes from the fact that the poles in a two-pole model are coupled to different channels. Indeed, gradually switching off the coupling between $\bar{K}N$ and $\pi\Sigma$ channels turns the upper pole into a real bound state in $\bar{K}N$, whereas the lower one

[1]After sending the present paper to the journal the results of the SIDDHARTA experiment appeared; see [21]. The 1σ SIDDHARTA region is situated inside the KEK square with comparable width Γ_{1s} and smaller level shift ΔE_{1s} values than those provided by our potentials.

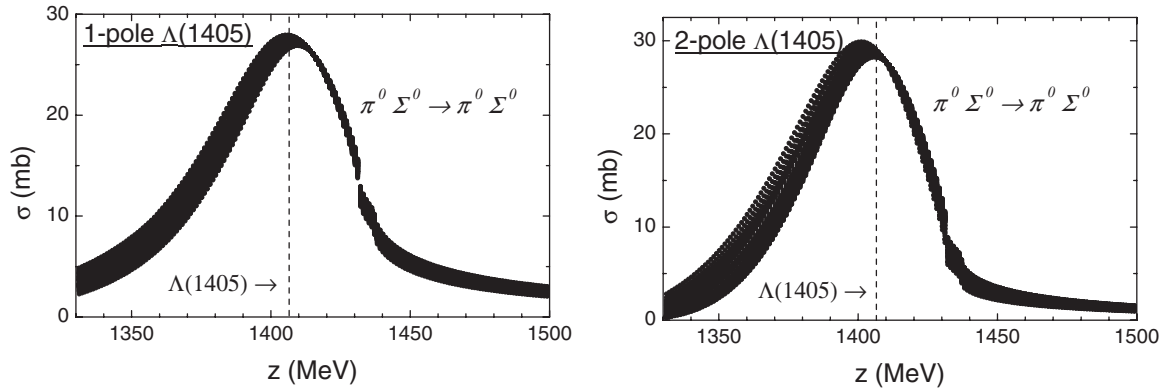

FIG. 4. Elastic $\pi^0\Sigma^0$ cross sections for the one-pole (left) and two-pole sets of the $\bar{K}N$-$\pi\Sigma$ potential. The theoretical bands are formed by all lines obtained with individual potentials within the corresponding set.

TABLE II. Parameters of the representative one- and two-pole $\bar{K}N$-$\pi\Sigma$ potentials: range $\beta^{\bar{\alpha}}$ (independent of two-body isospin I), strength $\lambda_I^{\bar{\alpha}\bar{\beta}}$, and additional parameter s of the two-pole model.

	$\beta^{\bar{K}N}$	$\beta^{\pi\Sigma}$	$\lambda_0^{\bar{K}\bar{K}}$	$\lambda_0^{\bar{K}\pi}$	$\lambda_0^{\pi\pi}$	$\lambda_1^{\bar{K}\bar{K}}$	$\lambda_1^{\bar{K}\pi}$	$\lambda_1^{\pi\pi}$	s
$V^{\text{one-pole}}_{\bar{K}N\text{-}\pi\Sigma}$	3.41	1.62	−1.2769	0.5586	0.2024	$1.0623 - i\,0.3251$	1.8315	1.7158	0.0000
$V^{\text{two-pole}}_{\bar{K}N\text{-}\pi\Sigma}$	3.72	1.00	−1.6588	0.4672	0.0072	$0.7329 - i\,0.2967$	1.5357	1.0744	−0.8433

becomes a resonance in the uncoupled $\pi\Sigma$ channel. Such a behavior was demonstrated in several papers (see, e.g., [3]). Accordingly, it was suggested that the poles of a two-body model manifest themselves in different reactions; in particular, $\bar{K}N$-$\bar{K}N$, $\bar{K}N$-$\pi\Sigma$, and $\pi\Sigma$-$\pi\Sigma$ amplitudes should "feel" only one of the two poles. We checked the hypothesis, and the results are demonstrated in Fig. 6. Indeed, real parts of $\bar{K}N$-$\bar{K}N$, $\bar{K}N$-$\pi\Sigma$, and $\pi\Sigma$-$\pi\Sigma$ amplitudes in the $I = 0$ state cross the real axis at different energies, but it is true for both versions of the potential. In fact, the difference is even larger for the one-pole amplitudes. In our opinion, the effect is caused by different background contributions in the reactions independently of the number of poles. Consequently, a proof of the two-pole structure of the $\bar{K}N$-$\pi\Sigma$ interaction does not exist.

The Coulomb interaction, directly included into the two-body Lippmann-Schwinger equations, was necessary for reproducing the experimental data on the kaonic hydrogen atom. However, in the K^-d scattering length calculations it is expected to play a minor role and can be omitted. We also neglected the difference between physical masses in isodoublets for the K^-d system. The physical characteristics of $\bar{K}N$-$\pi\Sigma$ system, calculated with isospin-averaged masses for $\bar{K}$ and N using the obtained sets of $\lambda_I^{\bar{\alpha}\bar{\beta}}$, $\beta_I^{\bar{\alpha}}$ parameters are shown in Figs. 3 and 7, and Table IV.

"Averaged" points $(\Delta E_{1s}, \Gamma_{1s})$ for the one- and two-pole representative potentials in Fig. 3 are shifted to the smaller $|\Delta E_{1s}|$ values relative to the "physical" ones. However, they remain inside the 1σ KEK region. Figure 7 demonstrates "averaged" and "physical" cross sections, where "averaged" ones naturally do not show threshold behavior at laboratory momentum P_{lab}, corresponding to the $\bar{K}^0n$ threshold. However, differences between "averaged" and "physical" cross sections are visible only in the near-threshold region, where there are no reliable experimental data.

TABLE III. Physical characteristics of the representative one-pole and two-pole potentials (full version with physical masses): strong pole(s) position(s) z_1 (and z_2), kaonic hydrogen $1s$ level shift ΔE_{1s} and width Γ_{1s}, K^-p scattering length a_{K^-p}, and threshold branching ratios γ and $R_{\pi\Sigma}$.

	$V^{\text{one-pole}}_{\bar{K}N\text{-}\pi\Sigma}$	$V^{\text{two-pole}}_{\bar{K}N\text{-}\pi\Sigma}$
z_1 (MeV)	$1409 - i36$	$1409 - i36$
z_2 (MeV)	–	$1381 - i105$
ΔE_{1s} (eV)	−377	−373
Γ_{1s} (eV)	434	514
a_{K^-p} (fm)	$-1.00 + i0.68$	$-0.96 + i0.80$
γ	2.36	2.36
$R_{\pi\Sigma}$	0.709	0.709

Finally, we see by comparing Table IV with Table III that strong pole positions remain almost unchanged. The scattering length a_{K^-p} changes for both versions of the potential mainly due to the confluence of the K^-p and $\bar{K}^0n$ thresholds into one $\bar{K}N$ threshold. Accordingly, threshold branching ratios γ (15) and $R_{\pi\Sigma}$ (16) are the only observables that are considerably changed after introducing isospin-averaged masses instead of physical ones.

B. Nucleon-nucleon potentials

Antisymmetrized three-body equations for the K^-d system with s-wave interactions contain only the spin-triplet NN interaction. We used different NN potentials in order to investigate the dependence of the K^-d scattering length on nucleon-nucleon interaction models. One of them is a two-term separable NN potential [24], which reproduces Argonne V18 [25] phase shifts and, therefore, is repulsive at short distances. The potential, which will be called TSA, is described by Eq. (13) with $N^{\bar{\alpha}} = 2$ and $\bar{\alpha} = \bar{\beta} = 1$ (since the NN interaction is obviously a diagonal one in particle indices). Two versions of the potential (TSA-A and TSA-B) with slightly different form factors were used:

$$
\begin{aligned}
g^{A,NN}_{(m)}(k) &= \sum_{n=1}^{2} \frac{\gamma^{A}_{(m)n}}{\left(\beta^{A}_{(m)n}\right)^2 + k^2} \quad \text{for} \quad (m) = 1, 2, \\
g^{B,NN}_{(1)}(k) &= \sum_{n=1}^{3} \frac{\gamma^{B}_{(1)n}}{\left(\beta^{B}_{(1)n}\right)^2 + k^2}, \\
g^{B,NN}_{(2)}(k) &= \sum_{n=1}^{2} \frac{\gamma^{B}_{(2)n}}{\left(\beta^{B}_{(2)n}\right)^2 + k^2}.
\end{aligned}
\tag{19}
$$

TSA-A and TSA-B potentials in the $^3S_1$ state yield the following scattering lengths and effective radii:

$$a^A(np) = -5.402 \quad \text{fm}, \quad r^A_{\text{eff}}(np) = 1.754 \text{ fm}, \tag{20}$$

$$a^B(np) = -5.413 \quad \text{fm}, \quad r^B_{\text{eff}}(np) = 1.760 \text{ fm}, \tag{21}$$

and they give the correct binding energy of the deuteron, $E_{\text{deu}} = 2.2246$ MeV.

We also used a one-term PEST potential [Eq. (13) with $N^{\bar{\alpha}} = 1$] from Ref. [26], which is a separablization of the Paris model of the NN interaction. The strength parameter of

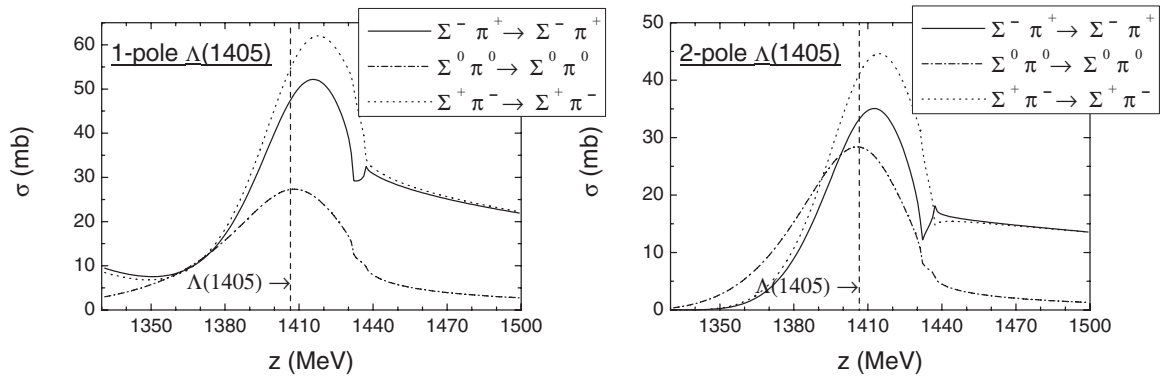

FIG. 5. Three charged elastic $\pi\Sigma$ cross sections for the representative one-pole (left) and two-pole $\bar{K}N$-$\pi\Sigma$ potentials.

PEST is $\lambda = -1$, and the form factor is defined by

$$g_I^{NN}(k) = \frac{1}{2\sqrt{\pi}} \sum_{n=1}^{6} \frac{c_{n,I}^{NN}}{k^2 + \left(\beta_{n,I}^{NN}\right)^2}, \tag{22}$$

where the constants $c_{n,I}^{NN}$ and $\beta_{n,I}^{NN}$ are listed in Ref. [26]. PEST is equivalent to the Paris potential on and off the energy shell up to $E_{\rm lab} \sim 50$ MeV. It reproduces the deuteron binding energy $E_{\rm deu} = 2.2249$ MeV, as well as the triplet and singlet NN scattering lengths, $a(^3S_1) = -5.422$ fm and $a(^1S_0) = 17.534$ fm, respectively.

The $^3S_1$ phase shifts for the three NN potentials are shown in Fig. 8 together with characteristics of the Argonne V18 model. Almost indistinguishable lines correspond to the two-term TSA-A and TSA-B potentials, which are very good at reproducing the Argonne V18 phase shifts. Their crossing of the real axis is a consequence of repulsion at short distances. The one-term PEST NN potential does not have such a property, but at low energies its phase shifts are also close to the "etalon" ones. Therefore, the two-term NN potentials, increasing the number of equations in a three-body system, reproduce properties of the NN interaction better than the one-term potential.

C. ΣN-ΛN interaction

The ΣN interaction, which is coupled with the ΛN channel in the $I = \frac{1}{2}$ isospin state, is usually assumed to be spin dependent [27,28]. We constructed new versions of the ΣN-ΛN potential in such a way that it reproduces existing experimental data [29–33]. One-term separable potentials, described by Eq. (13) with $N^{\bar{\alpha}} = 1$ and Yamaguchi form factors

$$g_{I,S}^{\Sigma N}(k) = \frac{1}{k^2 + \left(\beta_{I,S}^{\Sigma N}\right)^2} \tag{23}$$

were used for the two possible isospin states. But the number of channels is different for $I = \frac{1}{2}$ and $I = \frac{3}{2}$. The parameters of the one-channel ($\bar{\alpha} = \bar{\beta} = 1$) ΣN interaction with isospin $I = \frac{3}{2}$ were fitted to the $\Sigma^+ p \to \Sigma^+ p$ cross sections. Isospin one-half ΣN is coupled to the ΛN channel; therefore, at first we constructed a coupled-channel potential of the $I = \frac{1}{2}$ ΣN-ΛN interaction. The channel indices $\bar{\alpha}, \bar{\beta} = 1, 2$ in Eq. (13) denote the ΣN and ΛN channels, correspondingly. The coupled-channel $I = \frac{1}{2}$ potential together with the one-channel $I = \frac{3}{2}$ potential reproduces the $\Sigma^- p \to \Sigma^- p$, $\Sigma^- p \to \Sigma^0 n$, $\Sigma^- p \to \Lambda n$, and $\Lambda p \to \Lambda p$ cross sections.

Two versions of $I = \frac{1}{2}$ ΣN-ΛN and $I = \frac{3}{2}$ ΣN potentials were constructed: one, $V^{\rm Sdep}$, is spin dependent; the other, $V^{\rm Sind}$, is independent of spin. Both perfectly reproduce all existing experimental data [29–33] on ΣN and ΛN cross sections, as is seen in Fig. 9. Parameters of the potentials are shown in Table V together with scattering length values $a_{\frac{1}{2}}^{\Sigma N}$, $a_{\frac{3}{2}}^{\Sigma N}$, and $a_{\frac{1}{2}}^{\Lambda N}$. The scattering lengths of the spin-dependent potential $V^{\rm Sdep}$ are in qualitative agreement with those provided by more complicated models of the ΣN interaction [27,28]. The only exception is $a_{3/2}^{\Sigma N}$ with $S = 1$, having opposite sign, which, however, is the same as that given in previous versions of the same advanced potentials (notice that our definition of the sign of the scattering length is opposite to those used in the mentioned articles). The scattering lengths of the spin-independent potential $V^{\rm Sind}$ are not in such good agreement, but, keeping in mind that the scattering length is not a directly measurable quantity, we do not consider this difference to be a serious defect.

For the three-body $K^- d$ calculations, however, where a channel containing Λ is not included directly, we need not a coupled-channel but a one-channel ΣN model of interaction in the $I = \frac{1}{2}$ state. Due to this, we additionally constructed exact optical $V^{\Sigma N,{\rm Opt}}$ and simple complex $V^{\Sigma N,{\rm Complex}}$ potentials, corresponding to the obtained $I = \frac{1}{2}$ ΣN-ΛN potential. As was discussed at the beginning of Sec. III, the exact optical potential has an energy-dependent strength parameter defined by Eq. (14) and exactly reproduces the elastic ΣN amplitude of the corresponding two-channel potential. Parameters of $V^{\Sigma N,{\rm Complex}}$ were found in such a way that the simple complex potential gives the same scattering lengths as the two-channel potential. Thus, the exact optical and the simple complex ΣN(ΛN) potentials in the $I = \frac{1}{2}$ state and the one-channel ΣN potential in the $I = \frac{3}{2}$ were used during the three-body calculations. The second channel in brackets (ΛN) underlines that the one-channel potentials correspond to the coupled-channel one.

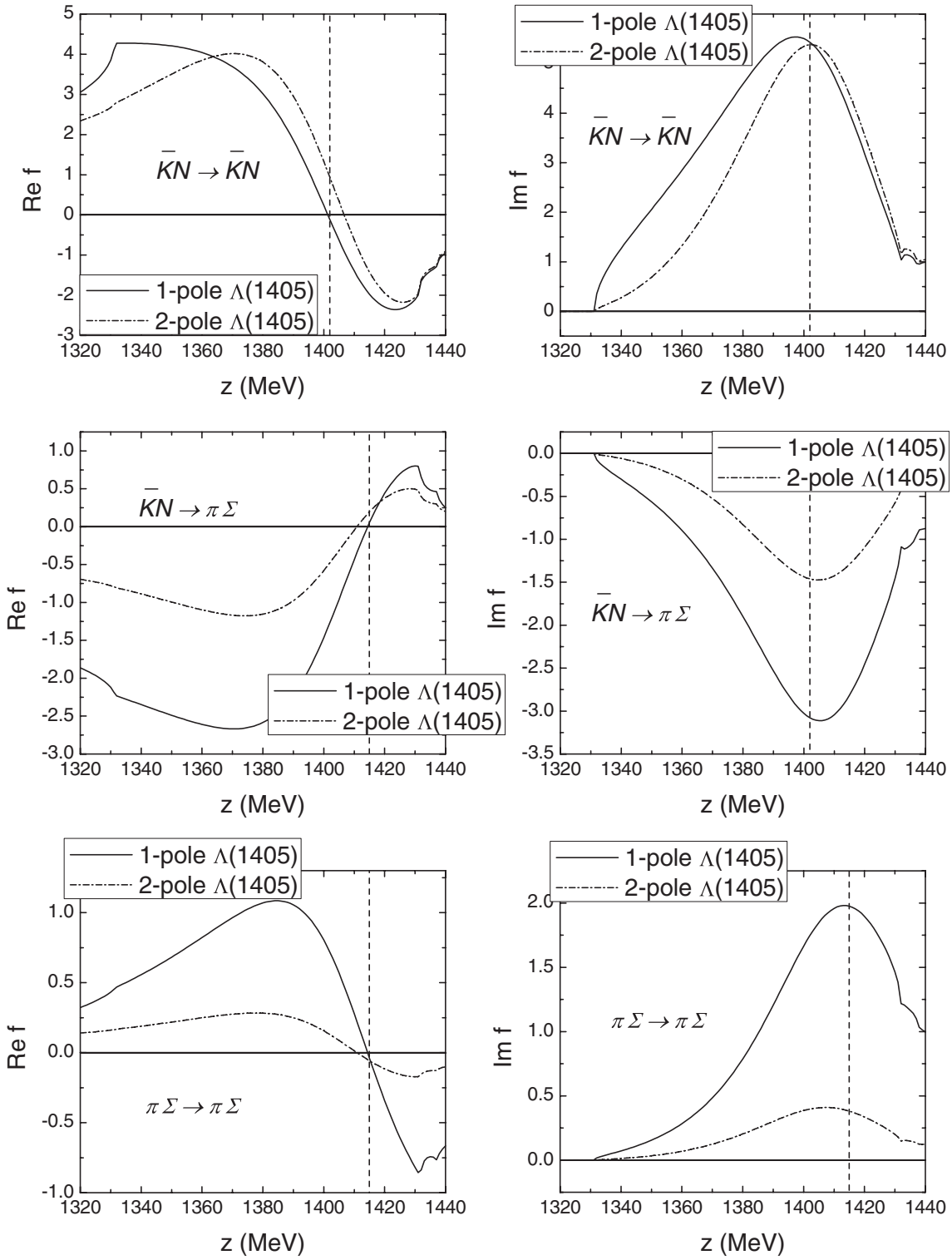

FIG. 6. Real (left column) and imaginary (right column) parts of the $\bar{K}N$-$\bar{K}N$, $\bar{K}N$-$\pi\Sigma$, and $\pi\Sigma$-$\pi\Sigma$ amplitudes obtained with one-pole (solid line) and two-pole (dash-dotted line) representative $\bar{K}N$-$\pi\Sigma$ potentials. The energies at which real parts of the one-pole amplitudes cross the real axes are denoted by vertical dashed lines.

IV. APPROXIMATE METHODS

Apart from the full coupled-channel calculation, we performed checks of several approximate methods, usually used for the K^-d scattering length problem, as well. It is obvious that a comparison between the full and approximate results is meaningful only if it is performed with equal two-body input.

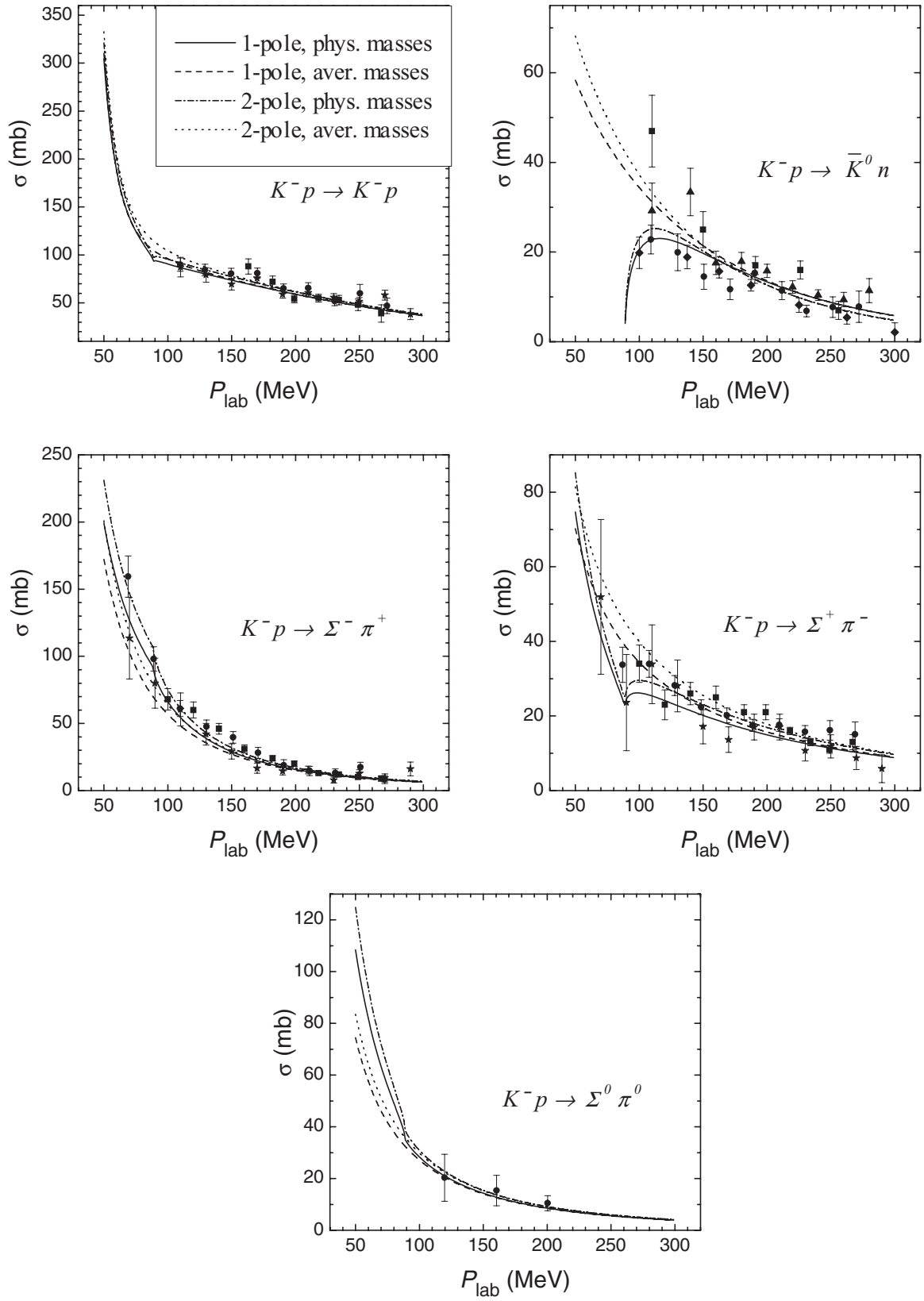

FIG. 7. Comparison of the theoretical $K^- p$ cross sections for the representative one- and two-pole $\bar{K}N$-$\pi\Sigma$ potentials with experimental data [13–17] (data points). The results obtained with the physical masses (solid, dash-dotted line) and the averaged masses (dashed and dotted line) are presented.

TABLE IV. The same as in Table III, but with averaged masses of the particles.

	$V^{\text{one-pole}}_{\bar{K}N\text{-}\pi\Sigma}$	$V^{\text{two-pole}}_{\bar{K}N\text{-}\pi\Sigma}$
z_1 (MeV)	$1409 - i36$	$1409 - i36$
z_2 (MeV)	–	$1381 - i105$
ΔE_{1s} (eV)	-316	-295
Γ_{1s} (eV)	414	491
a_{K^-p} (fm)	$-0.80 + i0.62$	$-0.72 + i0.73$
γ	4.18	4.54
$R_{\pi\Sigma}$	0.761	0.768

A. One-channel AGS calculations

In order to investigate the importance of direct inclusion of the $\pi\Sigma N$ channel we performed one-channel AGS calculations as well. This means that we solved Eq. (10) with $\alpha = \beta = 1$, and, thus, only $\bar{K}N$ and NN T matrices enter the equations. We constructed the exact optical and two simple complex one-channel $\bar{K}N(\text{-}\pi\Sigma)$ potentials approximating the full coupled-channel one- and two-pole models of interaction. As mentioned at the beginning of Sec. III, the exact optical potential $V^{\bar{K}N,\text{Opt}}$ provides exactly the same elastic $\bar{K}N$ amplitude as the coupled-channel model of interaction. Its energy-dependent strength parameters are defined by Eq. (14) with $\bar{\alpha}, \bar{\beta} = 1, 2$ standing for $\bar{K}N$ and $\pi\Sigma$ channels, correspondingly.

For the simple complex potentials we used range parameters $\beta^{\bar{K}N}$ of the coupled-channel $\bar{K}N$- $\pi\Sigma$ models of interaction. The complex $\lambda_I^{11,\text{Complex}}$ constants were obtained in two ways. The first version of the simple complex $\bar{K}N$ potential $V^{\bar{K}N,\text{Complex}}_{(a,z)}$ reproduces the K^-p scattering length a_{K^-p} and pole position z_1 of the corresponding coupled-channel version of the potential shown in Table IV. The second one, $V^{\bar{K}N,\text{Complex}}_{(a,a)}$, provides the same $I = 0$ and $I = 1$ isospin $\bar{K}N$ scattering lengths as the full $\bar{K}N$-$\pi\Sigma$:

$$a^{\text{one-pole}}_{\bar{K}N,I=0} = -1.60 + i\,0.67 \text{ fm},$$
$$a^{\text{two-pole}}_{\bar{K}N,I=0} = -1.62 + i\,0.78 \text{ fm}, \quad (24)$$

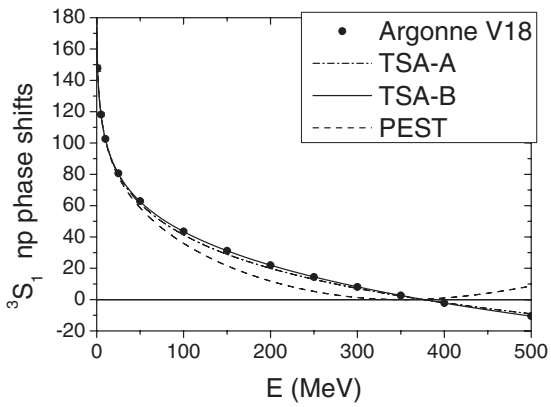

FIG. 8. $^3S_1$ np phase shifts of TSA-A (dash-dotted line), TSA-B (solid line), and PEST (dashed line) NN potentials in comparison with those of the Argonne V18 potential (solid circles).

$$a^{\text{one-pole}}_{\bar{K}N,I=1} = -0.004 + i\,0.57 \text{ fm},$$
$$a^{\text{two-pole}}_{\bar{K}N,I=1} = 0.18 + i\,0.68 \text{ fm}. \quad (25)$$

B. Fixed-center approximation

The so-called fixed-center approximation (FCA) to the Faddeev equations introduced in Ref. [34] is a variant of the fixed-scatterer approximation (FSA) or a two-center formula. In the FSA or two-center problem one assumes that the scattering of a projectile particle takes place on two much heavier target particles separated by a fixed distance. The motion of the heavy particles is subsequently taken into account by averaging the obtained projectile-target amplitude over the bound-state wave function of the target. Therefore, the approximation is well known and works properly in atomic physics, where an electron is really much lighter than a nucleon or an ion. Keeping in mind that the antikaon mass is just half the mass of a nucleon, we can hardly expect the FSA to be a good approximation for the K^-d scattering length calculation.

The FCA formula was obtained in Ref. [34] from the Faddeev equations in a very strange way. Proper derivation of a FSA formula starting from the same equations was done much earlier in Ref. [35]; it can also be found in Ref. [36] together with several versions of the FSA formula. The fixed-scatterer approximation for the calculation of the a_{K^-d} scattering length using separable potentials was used in Ref. [37].

A novelty of the FCA formula of [34] is the introduction of "isospin breaking terms," which, according to the authors, come from the $\bar{K}^0n$ two-body particle channel introduced in addition to K^-p. However, the inclusion of the $\bar{K}^0n$ channel is questionable, since, as was already mentioned in Sec. II, all terms connected with this subsystem automatically drop out from the Faddeev system of equations after antisymmetrization.

The necessity to go beyond the FCA formula for the K^-d system was clearly demonstrated in Ref. [8], where the unstable character of the FCA results was pointed out. However, the formula is still being used, for example in Ref. [38], which is why we decided to check the approximation. We used the same two-body input as in the AGS equations in order to make the comparison as adequate as possible.

First, we used the scattering lengths provided by our coupled-channel $\bar{K}N$-$\pi\Sigma$ potentials and the deuteron wave function corresponding to our TSA-B NN potential in the FCA formula, Eq. (24), from [34]. Second, all $\bar{K}^0n$ parts were removed from the formula because they do not enter the AGS equations. Finally, we took into account the fact that the FCA formula was obtained for a local $\bar{K}N$ potential, while separable $\bar{K}N$-$\pi\Sigma$ potentials were used in our Faddeev equations. The corresponding changes in the FCA formula were made.[2] Therefore, the two-body input for the FCA formula was equivalent to the input for the AGS calculation.

[2]To remove the difference we used the function $G(R)$ defined by Eq. (25) in Ref. [37] instead of the function $1/R$, which is an approximation of $G(R)$ in the FCA formula. The range parameter

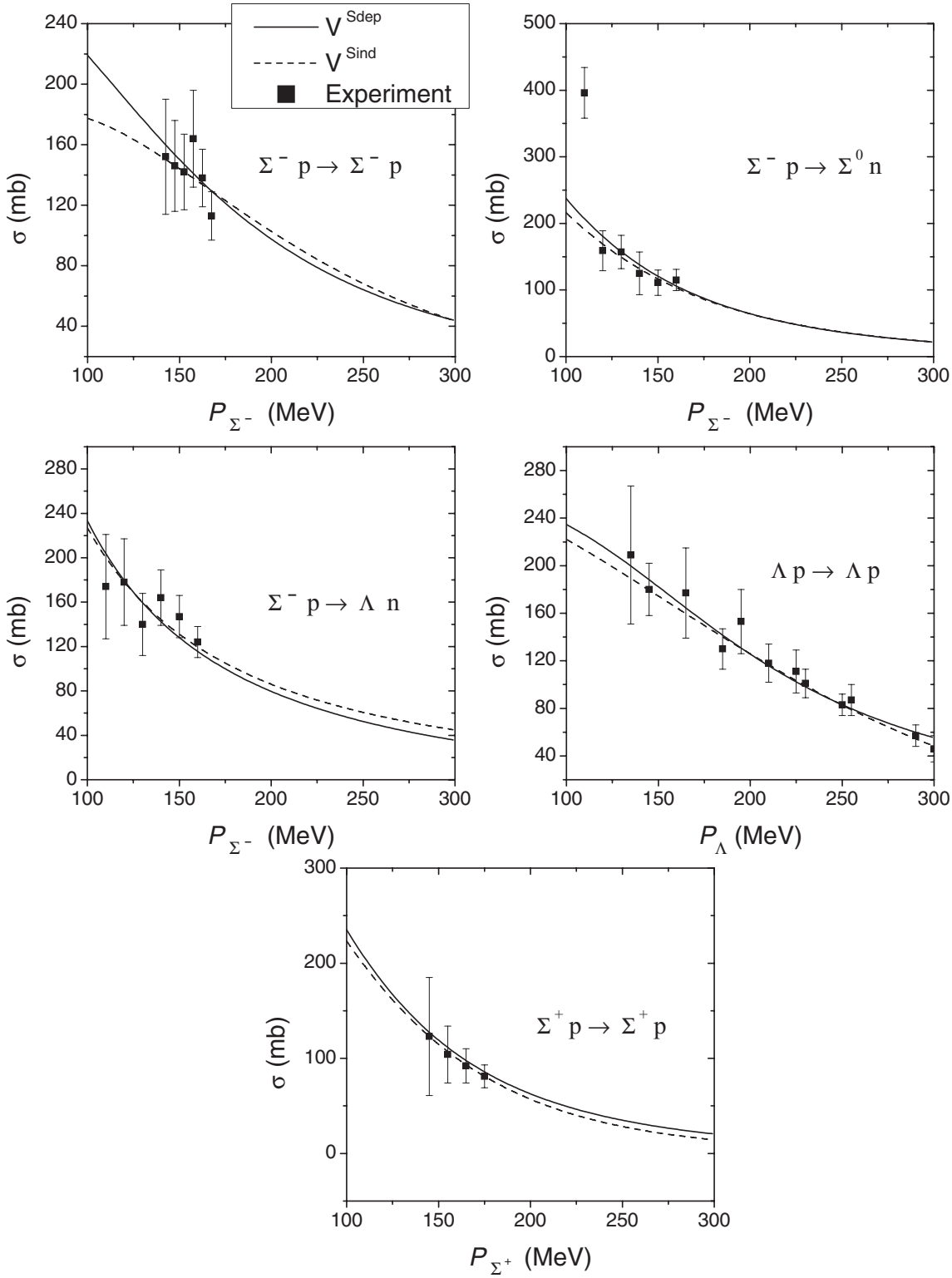

FIG. 9. Comparison of several theoretical cross sections for the spin-dependent (solid line) and spin-independent (dashed line) coupled-channel ΣN-ΛN potentials with experimental data [29–33] (data points).

V. RESULTS AND DISCUSSION

The results of the full coupled-channel calculations of the $K^- d$ scattering length using sets of one-pole (empty circles) and two-pole (empty squares) versions of the coupled-channel

$\beta^{\bar{K}N}$, entering the $G(R)$ function, was also taken from our coupled-channel $\bar{K}N$-$\pi\Sigma$ potential. In fact, the replacement of $1/R$ by $G(R)$ changed the results negligibly.

TABLE V. Range $\beta^{\bar{\alpha}}$ (independent of two-body isospin I) and strength $\lambda_I^{\bar{\alpha}\bar{\beta}}$ parameters of the two ΣN-ΛN potentials: $V_S^{\rm Sdep}$ and $V^{\rm Sind}$ (where S stands for the spin). Scattering lengths $a_I^{\bar{\alpha}}$ of ΣN and ΛN systems are also shown (in femtometers).

	$\beta^{\Sigma N}$	$\lambda_{\frac{3}{2}}^{\Sigma N}$	$\beta^{\Lambda N}$	$\lambda_{\frac{1}{2}}^{\Sigma\Sigma}$	$\lambda_{\frac{1}{2}}^{\Sigma\Lambda}$	$\lambda_{\frac{1}{2}}^{\Lambda\Lambda}$	$a_{\frac{1}{2}}^{\Sigma N}$	$a_{\frac{3}{2}}^{\Sigma N}$	$a_{\frac{1}{2}}^{\Lambda N}$
$V_{S=0}^{\rm Sdep}$	1.25	−0.0244	0.62	−1.9956	1.1408	−0.7148	$-1.90 + i\,0.08$	3.18	1.26
$V_{S=1}^{\rm Sdep}$	0.50	−0.0007	1.03	−0.0008	0.0185	0.0000	$-3.17 + i\,1.30$	1.63	1.57
$V^{\rm Sind}$	0.74	−0.0032	0.74	−0.0011	0.0254	0.0190	$-2.40 + i\,0.85$	1.95	−1.47

$\bar{K}N$-$\pi\Sigma$ potentials are shown in Fig. 10 . The calculations were performed with $V_{NN}^{\rm TSA-B}$ and the exact optical potential $V_{\Sigma N}^{\rm Sdep,Opt}$. The K^-p scattering length values obtained with the two representative $\bar{K}N$-$\pi\Sigma$ potentials are

$$a_{K^-d}^{\text{one-pole}} = -1.49 + i\,0.98 \text{ fm}, \quad (26)$$

$$a_{K^-d}^{\text{two-pole}} = -1.57 + i\,1.11 \text{ fm}. \quad (27)$$

Results of previous Faddeev calculations of the same system (filled squares) together with two FCA results (crossed squares) are also shown in the figure.

It is seen that the sets of a_{K^-d} results obtained with one- and two-pole versions of "the main" $\bar{K}N$-$\pi\Sigma$ interaction are clearly separated from one another. Thus, in principle, it would be possible to favor one version of the $\bar{K}N$-$\pi\Sigma$ potential by comparing with an experimental result. However, it is not absolutely clear whether the difference between the two sets is much more than theoretical uncertainties, caused mainly by the uncertainties of the models of the $\bar{K}N$ interaction. Moreover, direct measurement of the K^-d scattering length is impossible. Therefore, a calculation of the $1s$ level shift $\Delta E_{\rm deu,1s}$ and width $\Gamma_{\rm deu,1s}$ of the kaonic deuterium atom, corresponding to the obtained a_{K^-d} values, is necessary for comparison with eventual experimental data. The characteristics of kaonic deuterium were being measured by the SIDDHARTA experiment—unfortunately, without any

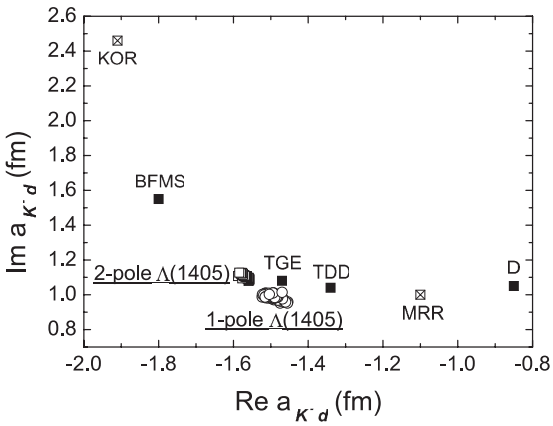

FIG. 10. The results of the full K^-d scattering length calculations using sets of one-pole (empty circles) and two-pole (empty squares) versions of $\bar{K}N$-$\pi\Sigma$ potential. Previous Faddeev calculations—BFMS [8], TGE [39], TDD [40], and D [41] (filled squares)— and FCA results—KOR [34] and MRR [38] (crossed squares)— are also shown.

results. Due to this, our next step will consist in making predictions for $\Delta E_{\rm deu,1s}$ and $\Gamma_{\rm deu,1s}$ observables.

As is seen in Fig. 10, our a_{K^-d} results are close to the other K^-d scattering lengths obtained in Refs. [39,40] within the coupled-channel Faddeev approach. The result of [41], obtained using a one-channel Faddeev calculation with a zero-range one-channel $\bar{K}N$ potential, has much smaller absolute value of the real part than all other a_{K^-d} values. In contrast, the authors of Ref. [8], who performed Faddeev calculations using the NN interaction with a d-wave component, obtained a K^-d scattering length with rather larger absolute values of both real and imaginary parts.

The a_{K^-d} value of [34], which is significantly different from all others, was calculated using the FCA formula obtained in the same paper and already discussed in Sec. IV B. We chose the result calculated in the isospin basis for the comparison. One more paper in which the FCA formula was used is [38]; there, however, the result was obtained by simply applying two approximate formulas. The second one is the corrected Deser formula, used for calculation of the $\bar{K}N$ scattering lengths entering the FCA. One of the representative a_{K^-d} values from [38], having the largest possible imaginary part, is shown in Fig. 10.

It is hard to compare all a_{K^-d} results, because the methods of treatment of the three-body problem and two-body inputs are different in the mentioned works. In order to investigate separate effects of several approximations we performed approximate calculations, as described in Sec. IV. The obtained one-channel AGS a_{K^-d} values (Sec. IV A) together with FCA (Sec. IV B) and the representative coupled-channel AGS results of the K^-d scattering length calculations are shown in Fig. 11 for one- and two-pole versions of the $\bar{K}N$-$\pi\Sigma$ interaction. It is important that all results in the figure were obtained with equivalent two-body input, including the neglect of isospin-breaking parts in the original FCA formula.

It is seen from Fig. 11 that all approximations are more accurate for the one-pole version of the $\bar{K}N$ interaction than for the two-pole variant. The one-channel AGS calculation with the exact optical $\bar{K}N$ potential (empty symbols), giving exactly the same $\bar{K}N$-$\bar{K}N$ amplitude as the corresponding coupled-channel potential, turns out to be the best approximation. The result, obtained with the simple complex potential $V_{(a,a)}^{\bar{K}N,\rm Complex}$ (vertically crossed symbols), reproducing $I = 0$ and $I = 1$ $\bar{K}N$ scattering lengths, underestimates the absolute value of the real part of a_{K^-d}, especially for the two-pole version of the $\bar{K}N$ interaction, but has a rather accurate imaginary part of the K^-d scattering length. Another one-channel AGS calculation with simple complex potential $V_{(a,z)}^{\bar{K}N,\rm Complex}$, reproducing the

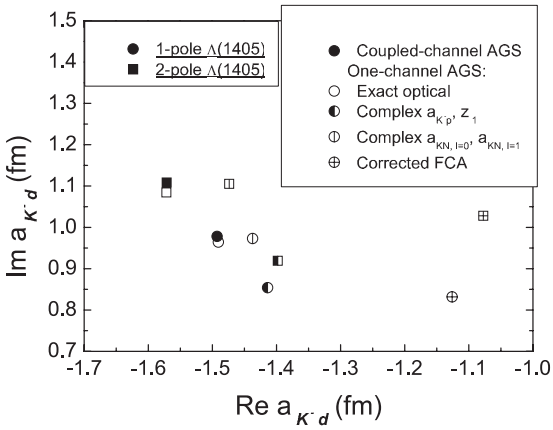

FIG. 11. Comparison of the full results of the a_{K^-d} calculations with representative one-pole (circles) and two-pole (squares) versions of the $\bar{K}N$-$\pi\Sigma$ potential with approximate results. Values obtained with coupled-channel AGS equations (filled symbols), one-channel AGS with the exact optical $\bar{K}N$ potential $V^{\bar{K}N,\mathrm{Opt}}$ (empty symbols), one-channel AGS with complex $V^{\bar{K}N,\mathrm{Complex}}_{(a,z)}$ (half-empty symbols), and $V^{\bar{K}N,\mathrm{Complex}}_{(a,a)}$ (vertically crossed symbols) are shown. Results of the corrected FCA formula (crossed symbols) are also shown.

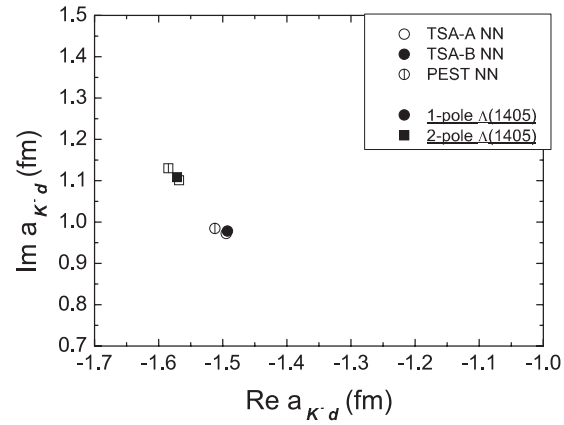

FIG. 12. Dependence of the full K^-d scattering length results on the NN interaction: a_{K^-d} obtained with TSA-A (empty symbols), TSA-B (filled symbols), and PEST (vertically crossed symbols) NN potentials. One-pole (circles) and two-pole (squares) representative versions of the $\bar{K}N$-$\pi\Sigma$ interaction were used.

K^-p scattering length and pole position z_1, gives a rather inaccurate result (half-empty symbols) as compared with the coupled-channel AGS values (filled symbols).

The scattering length a_{K^-d} of [41] was obtained from the one-channel Faddeev equations with a complex potential. However, the underestimation of the absolute values of its real part in comparison to other Faddeev calculations is so large that it cannot be explained by the method only. The most likely reason for the difference lies in the properties of the $\bar{K}N$ potential used in Ref. [41]. First of all, the potential gives a very large mass for the K^-p quasibound state (1439 MeV), which, therefore, is situated above the K^-p threshold. In addition, the width of the state (127 MeV) is much larger than the PDG value (50 MeV) as well as the width of our z_1 pole (72 MeV).

It is hard to understand the results obtained in Ref. [8]. While all formulas are written for many-channel Faddeev equations, most of the dependencies and even "the best" a_{K^-d} value were obtained within a one-channel Faddeev calculation including $\bar{K}N$ and NN interactions only. Since the elastic part of the coupled-channel $\bar{K}N$ T matrix was used, the result is equivalent to a one-channel Faddeev calculation with an exact optical potential. But even the full coupled-channel calculation was performed in Ref. [8] with nonunitary $\bar{K}N$ T matrices OSA and OS1, since channels with η mesons, entering the two-body T, were omitted in the three-body equations. It is not clear why the one-channel calculations of [8] give so large a difference in imaginary parts of a_{K^-d} obtained in the isospin and the particle basis and with and without the d-wave in NN. The result of a calculation, in principle, should not depend on the chosen basis; in addition, the very recent results of K^-d scattering calculations [42] demonstrated that inclusion of physical masses into the Faddeev equations changes a_{K^-d} by several percents only.

The results of using the FCA formula without isospin-breaking effects (crossed symbols) stays far away from the full calculation, as is seen in Fig. 11. While errors for the imaginary part are not so large, the modulus of the real part is underestimated by about 30%. Therefore, our calculations show that the FCA is a poor approximation for the K^-d scattering length calculation, and the accuracy is lower for the two-pole $\bar{K}N$ model of interaction (notice that most chirally based models of the $\bar{K}N$ interaction have two-pole structure). Even the original FCA formula does not give such a large K^-d scattering length as a_{K^-d} from [34], which, therefore, is caused by input $\bar{K}N$ scattering lengths that are too large. As for the values of [38], they suffer from cumulative errors of two approximations and using of DEAR results on kaonic hydrogen characteristics. As was shown in Ref. [3], the error of the corrected Deser formula amounts to about 10%, while the problems with DEAR experimental data were also demonstrated in the paper and in other theoretical works.

We investigated the dependence of the full coupled-channel results on NN and $\Sigma N(\text{-}\Lambda N)$ interactions as well. The dependence of a_{K^-d} on the nucleon-nucleon interaction is demonstrated in Fig. 12 , where the results obtained with TSA-A, TSA-B, and PEST V^{NN} are shown. The representative sets of one- and two-pole $\bar{K}N$-$\pi\Sigma$ potentials were used together with the exact optical $V^{\mathrm{Sdep,Opt}}\Sigma N(\text{-}\Lambda N)$ model of interaction. We see from the figure that the difference is very small even for the potentials with and without repulsion at short distances (TSA and PEST, correspondingly). Therefore, the s-wave NN interaction, which is used in the present calculation, plays a minor role in the calculation. Most likely, it is caused by relative weakness of the NN interaction as compared to $\bar{K}N$ from the viewpoint of a much deeper quasibound state in the latter system ($E_{\bar{K}N} \approx 23$ MeV for our potentials) than in the deuteron bound state ($E_{\mathrm{deu}} \approx 2$ MeV). We do not expect a much larger effect from higher partial waves in NN as well.

We also looked at the dependence of a_{K^-d} on the $\Sigma N(-\Lambda N)$ interaction. The K^-d scattering lengths obtained with the exact optical and the simple complex versions of the spin-dependent V^{Sdep} and spin-independent V^{Sind} potentials are shown in Fig. 13. The representative sets of one- and

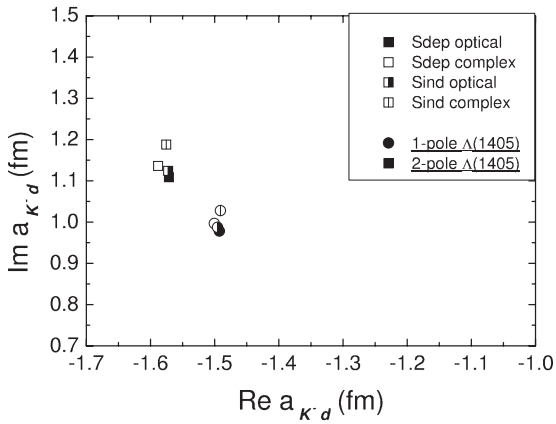

FIG. 13. Dependence of the full K^-d scattering length results on the ΣN-(ΛN) interaction. The a_{K^-d} values obtained with the exact optical $V^{\mathrm{Sdep,Opt}}$ (filled square), simple complex $V^{\mathrm{Sdep,Complex}}$ (empty square), exact optical $V^{\mathrm{Sind,Opt}}$ (half-empty square), and simple complex $V^{\mathrm{Sind,Complex}}$ (vertically crossed square) ΣN-(ΛN) potentials are shown. One-pole (circles) and two-pole (squares) representative versions of the $\bar{K}N$-$\pi\Sigma$ interaction were used.

two-pole $\bar{K}N$-$\pi\Sigma$ potentials were used together with the TSA-B NN potential. The results of the two versions of the ΣN-(ΛN) potential V^{Sdep} and V^{Sind} in exact optical form are very close, while their simple complex versions are slightly different. However, the largest error does not exceed 3%; therefore, the dependence of a_{K^-p} on the ΣN-(ΛN) interaction is also weak.

VI. CONCLUSIONS

To conclude, we performed calculations of the K^-d scattering length using newly obtained coupled-channel $\bar{K}N$-$\pi\Sigma$ potentials with one- and two-pole versions of the $\Lambda(1405)$ resonance. Faddeev-type AGS equations were used for description of the $\bar{K}NN$-$\pi\Sigma N$ system. We also constructed new coupled-channel ΣN-ΛN potentials together with its exact optical and simple complex ΣN-(ΛN) versions. Different models of the NN interaction—TSA-A, TSA-B, and PEST—were used. All two-body interactions are described by s-wave separable potentials. We investigated the dependence of a_{K^-d} on the NN and the ΣN-(ΛN) interactions and found that both dependencies are weak.

We found that the two sets of results, obtained with one- and two-pole models of the $\Lambda(1405)$ resonance, are clearly separated from one another, in principle, allowing us to give preference to one of the $\bar{K}N$-$\pi\Sigma$ interaction models. However, the question of whether theoretical uncertainties are not of the same order as the differences between the two obtained sets of a_{K^-d} remains open. In any case, it is necessary to calculate level shifts and widths of the kaonic deuterium atom, corresponding to the obtained K^-d scattering lengths, which can be measured, say, by the SIDDHARTA-2 experiment. This is expected to be done in a follow-up paper.

Among the approximate results, the one-channel AGS calculation with the exact optical $\bar{K}N$-$(\pi\Sigma)$ potential gives the best approximation to the full coupled-channel result. In contrast, the FCA was shown to be the least-accurate approximation, especially in reproduction of the real part of the K^-d scattering length. All approximations are less accurate for the two-pole model of the $\bar{K}N$-$\pi\Sigma$ interaction.

ACKNOWLEDGMENTS

The author is grateful to J. Révai for many fruitful discussions and to J. Haidenbauer for his comments concerning ΣN-ΛN interaction. The work was supported by the Czech GA AVCR Grant No. KJB100480801.

[1] Mini-Proceedings ECT* Workshop (ECT*, Trento, Italy, October 12–16, 2009), edited by C. Curceanu and J. Marton, arXiv:1003.2328 [nucl-ex].
[2] L. D. Faddeev, Zh. Eksp. Theor. Fiz. **39**, 1459 (1960) [Sov. Phys. JETP **12**, 1014 (1961)].
[3] J. Révai and N. V. Shevchenko, Phys. Rev. C **79**, 035202 (2009).
[4] C. Curceanu *et al.*, Eur. Phys. J. A **31**, 537 (2007).
[5] N. V. Shevchenko, A. Gal, and J. Mareš, Phys. Rev. Lett. **98**, 082301 (2007).
[6] N. V. Shevchenko, A. Gal, J. Mareš, and J. Révai, Phys. Rev. C **76**, 044004 (2007).
[7] E. O. Alt, P. Grassberger, and W. Sandhas, Nucl. Phys. B **2**, 167 (1967).
[8] A. Bahaoui, C. Fayard, T. Mizutani, and B. Saghai, Phys. Rev. C **68**, 064001 (2003).
[9] V. B. Belyaev, *Lectures on the Theory of Few-Body Systems* (Springer Verlag, New York, 1990).
[10] F. Sohre and H. Ziegelman, Phys. Lett. B **34**, 579 (1971).
[11] D. N. Tovee *et al.*, Nucl. Phys. B **33**, 493 (1971).
[12] R. J. Nowak *et al.*, Nucl. Phys. B **139**, 61 (1978).
[13] M. Sakitt *et al.*, Phys. Rev. B **139**, 719 (1965).
[14] J. K. Kim, Phys. Rev. Lett. **14**, 29 (1965); Columbia University Report, Nevis, 149 (1966); J. K. Kim, Phys. Rev. Lett. **19**, 1074 (1967).
[15] W. Kittel, G. Otter, and I. Wacek, Phys. Lett. **21**, 349 (1966).
[16] J. Ciborowski *et al.*, J. Phys. G **8**, 13 (1982).
[17] D. Evans *et al.*, J. Phys. G **9**, 885 (1983).
[18] W. E. Humphrey and R. R. Ross, Phys. Rev. **127**, 1305 (1962).
[19] M. Iwasaki *et al.*, Phys. Rev. Lett. **78**, 3067 (1997); T. M. Ito *et al.*, Phys. Rev. C **58**, 2366 (1998).
[20] G. Beer *et al.*, Phys. Rev. Lett. **94**, 212302 (2005).
[21] M. Bazzi *et al.*, Phys. Lett. B **704**, 113 (2011).
[22] K. Nakamura *et al.* (Particle Data Group), J. Phys. G **37**, 075021 (2010).
[23] R. Schumacher (for the CLAS Collaboration), AIP Conf. Proc. **1257**, 100 (2010).
[24] P. Doleschall (private communication).
[25] R. B. Wiringa, V. G. J. Stoks, and R. Schiavilla, Phys. Rev. C **51**, 38 (1995).
[26] H. Zankel, W. Plessas, and J. Haidenbauer, Phys. Rev. C **28**, 538 (1983).
[27] J. Haidenbauer and U.-G. Meissner, Phys. Rev. C **72**, 044005 (2005).

[28] Th. A. Rijken and Y. Yamamoto, Phys. Rev. C **73**, 044008 (2006).
[29] G. Alexander, U. Karshon, A. Shapira, G. Yekutieli, R. Engelmann, H. Filthuth, and W. Lughofer, Phys. Rev. **173**, 1452 (1968).
[30] B. Sechi-Zorn, B. Kehoe, J. Twitty, and R. A. Burnstein, Phys. Rev. **175**, 1735 (1968).
[31] F. Eisele, H. Filthuth, W. Fölisch, V. Hepp, E. Leitner, and G. Zech, Phys. Lett. B **37**, 204 (1971).
[32] R. Engelmann, H. Filthuth, V. Hepp, and E. Kluge, Phys. Lett. **21**, 587 (1966).
[33] V. Hepp and M. Schleich, Z. Phys. **214**, 71 (1968).
[34] S. S. Kamalov, E. Oset, and A. Ramos, Nucl. Phys. A **690**, 494 (2001).
[35] V. V. Peresypkin, Ukr. J. Phys. **23**, 1256 (1978).
[36] A. Deloff, *Fundamentals in Hadronic Atom Theory* (World Scientific, Singapore, 2003).
[37] R. C. Barrett and A. Deloff, Phys. Rev. C **60**, 025201 (1999).
[38] U.-G. Meissner, U. Raha, and A. Rusetsky, Eur. Phys. J. C **47**, 473 (2006).
[39] G. Toker, A. Gal, and J. M. Eisenberg, Nucl. Phys. A **362**, 405 (1981).
[40] M. Torres, R. H. Dalitz, and A. Deloff, Phys. Lett. B **174**, 213 (1986).
[41] A. Deloff, Phys. Rev. C **61**, 024004 (2000).
[42] J. Révai (private communication).